ELSEVIER

Tectonophysics 336 (2001) 19–30

TECTONOPHYSICS

www.elsevier.com/locate/tecto

# Implications of hydrostatic pore pressures and high crustal strength for the deformation of intraplate lithosphere

Mark D. Zoback, John Townend*

*Department of Geophysics, Stanford University, Stanford, CA 94305-2215, USA*

**Abstract**

Observations from deep boreholes at several locations worldwide indicate that (i) hydrostatic pore pressures persist to depths of as much as 12 km in the upper crust, (ii) the brittle crust is in a state of failure equilibrium according to Coulomb frictional-failure theory, and (iii) bulk permeability is high — $10^{-17}$–$10^{-16}$ $m^2$ — apparently due to fluid flow along critically stressed faults. As a result of these factors, the brittle crust is stronger than it would be under near-lithostatic pore pressure conditions.

This result provides a constraint on models of lithospheric deformation. Postulating that the upper and lower crust and lithospheric mantle are totally coupled and that the total strength of the lithosphere is equal to the magnitude of tectonic driving forces ($\sim 3 \times 10^{12}$ N $m^{-1}$), we have calculated lithospheric strain rates under representative thermal and rheological conditions such that the integrated differential stress over the entire thickness of the lithosphere equals the plate driving force. For a strike-slip stress state and surface heat flow of $60 \pm 6$ mW $m^{-2}$, average strain rates are approximately $10^{-18}$ $s^{-1}$ under hydrostatic upper crustal pore pressure conditions, and approximately $10^{-15}$ $s^{-1}$ under near-lithostatic pore pressures. The latter strain rates are higher than either observed geodetically using very long baseline interferometry (VLBI), or estimated on the basis of plate tectonic reconstructions. Hence we argue that hydrostatic upper crustal pore pressures enable lithospheric plates to behave rigidly over time scales of tens to hundreds of millions of years. 

*Keywords*: crustal strength; fault mechanics; intraplate lithosphere; pre pressure; strain rate; stress

## 1. Introduction

From a purely theoretical perspective, the estimated strength of intraplate continental crust varies widely. Analyses of lithospheric flexure indicate that the strength is high (e.g. McNutt, 1984) and the crust can support differential stresses of several hundred megapascals. In contrast, modeling of lithospheric deformation using thin viscous sheet models suggests that the strength of the crust may be quite low over geologic time periods (e.g. Houseman and England, 1986; England and Houseman, 1986). In this paper, we investigate upper crustal strength and its relation to intraplate deformation.

It is well known that the frictional strength of the crust depends not only on the intrinsic frictional strength of faulted rock, but also on the pore pressure at depth (Hubbert and Rubey, 1959). As pointed out by numerous authors, combining Coulomb frictional-failure theory (e.g. Jaeger and Cook, 1979) with laboratory-derived coefficients of friction (Byerlee, 1978) leads to the conclusion that the brittle strength of the crust is of the order of several hundred megapascals under hydrostatic pore pressure conditions and vanishingly small as pore pressures approach

* Corresponding author. Tel.: +1-650-723-4746; fax: +1-650-723-7344.

*E-mail address:* jtownend@stanford.edu (J. Townend).

0040-1951/01/$ - see front matter 
PII: S0040-1951(01)00091-9

lithostatic values (Sibson, 1974; Brace and Kohlstedt, 1980).

The cumulative strength of the lithosphere is the sum of the brittle strength of the upper crust and the viscous strength of the lower crust and upper mantle. From considerations of tectonic driving forces (slab pull and ridge push), thrust zone topography, and elastic plate deformation, several authors have estimated the total force available to drive lithospheric deformation to be approximately $1–4 \times 10^{12}$ N m$^{-1}$ (Forsyth and Uyeda, 1975; Bott and Kusznir, 1984; Kusznir, 1991).

In this paper, we investigate the effects of crustal pore pressure regimes on estimated lithospheric strain rates, subject to the constraint that the total force acting on the lithosphere is $3 \times 10^{12}$ N m$^{-1}$. As discussed by Liu and Zoback (1997), maximum intraplate lithospheric strain rates can be estimated using the constraint that the cumulative strength of the lithosphere,

$$S_L = \int_0^D \Delta S \, dz \tag{1}$$

(England and Houseman, 1986), is equal to the available plate driving force, where $D$ is the thickness of the lithosphere and $\Delta S$ is the differential stress. The manner in which the plate driving force is related to lithospheric deformation can be investigated using strength envelopes, incorporating appropriate rheologies to represent the ductile behavior of the lower crust and lithospheric mantle. A test of such models is that the estimated intraplate lithospheric strain rate not exceed approximately $10^{-17}$ s$^{-1}$, in order to be consistent with plate tectonic reconstructions (J. Morgan, unpublished). For example, during the ~100 Ma duration of the Atlantic Ocean's opening, no more than approximately 100 km of shortening has taken place in the ~10 000 km-wide African or South American plates. Thus, the maximum *intraplate* strain rate is of the order of 100 km/(10 000 km × 100 Ma) ≈ $10^{-17}$ s$^{-1}$. Moreover, very long baseline interferometry (VLBI) measurements place an upper bound of $10^{-17}$ s$^{-1}$ on strain rates within the North American plate (Gordon, 1998), and average seismic strain rates in the eastern United States are $10^{-19}$–$10^{-18}$ s$^{-1}$ (Anderson, 1986). We conclude from this that intraplate continental lithosphere does not deform more rapidly than at strain rates of ~$10^{-17}$ s$^{-1}$ on geological time scales.

## 2. Implications of Coulomb frictional-failure theory for stress levels in the brittle crust

Three independent lines of evidence suggest that a state of failure equilibrium exists within intraplate continental upper crust: (i) seismicity induced by fluid injection (e.g. Raleigh et al., 1972; Pine et al., 1983; Zoback and Harjes, 1997) or reservoir impoundment (e.g. Simpson et al., 1988; Roeloffs, 1996); (ii) earthquakes triggering other earthquakes (e.g. Stein et al., 1992, 1997), and; (iii) in situ stress measurements in deep boreholes (e.g. Zoback and Healy, 1992; Brudy et al., 1997). Additionally, measured stresses are consistently found to be approximately equal to the stresses predicted using Coulomb frictional-failure theory (Pine et al., 1983; Zoback and Healy, 1984, 1992; Townend and Zoback, 2000) for laboratory-derived coefficients of friction of 0.6–1.0 (Byerlee, 1978).

The frictional strength of the brittle crust can be computed by consideration of a pre-existing, cohesionless fault whose normal is at an angle $\theta$ to the maximum compressive principal stress, $S_1$. The shear and effective normal stresses (tractions) on this fault are given, respectively, by

$$\tau = \frac{S_1 - S_3}{2} \sin 2\theta = \frac{\Delta S_{\text{brittle}}}{2} \sin 2\theta \tag{2}$$

and

$$\sigma_n = \frac{S_1 + S_3 - 2P_f}{2} + \frac{S_1 - S_3}{2} \cos 2\theta$$

$$= \bar{S} - P_f + \frac{\Delta S_{\text{brittle}}}{2} \cos 2\theta \tag{3}$$

where $S_3$ is the minimum principal stress, $P_f$ is the fluid pressure, and $\Delta S_{\text{brittle}}$ and $\bar{S}$ are the brittle differential stress and mean stress given by $S_1 - S_3$ and $(S_1 + S_3)/2$, respectively (Jaeger and Cook, 1979). If the plane is critically stressed, then

$$\tau = \mu \sigma_n = \sigma_n \tan \phi \tag{4}$$

This is referred to as the Coulomb frictional-failure criterion, in which $\mu = \tan \phi$ is the coefficient of friction and $\phi$ is referred to as the angle of friction. At failure, $\phi = 2\theta - \pi/2$ and the plane is referred to as 'optimally oriented'. Combining Eq. (2)–(4), gives

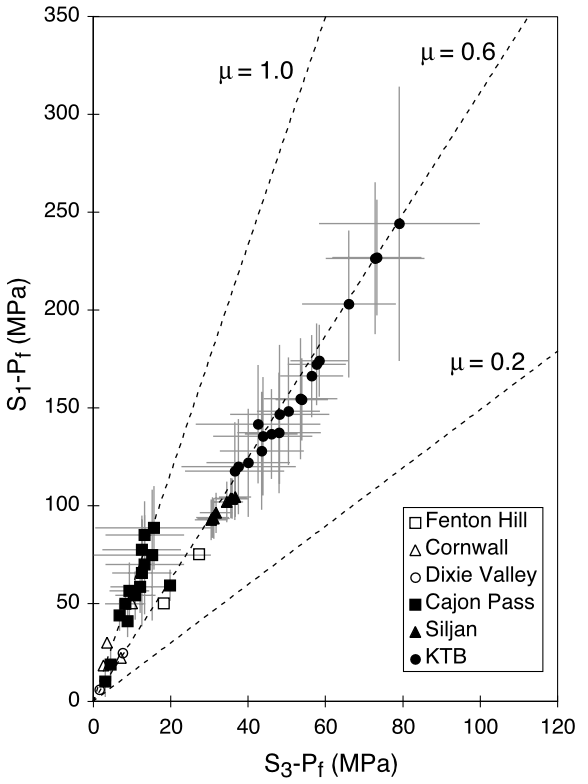


Fig. 1. Stress data from six of the boreholes listed in Table 1 illustrating that the upper crust is in a stress state consistent with that predicted using Coulomb frictional-failure theory (Eq. (5)) incorporating frictional coefficients of approximately 0.6–1.0. Error bars have not been plotted for the smaller datasets for the sake of clarity. Sources: Pine et al. (1983), Batchelor and Pine (1986), Barton et al. (1988), Zoback and Healy (1992), Hickman et al. (1997), Brudy et al. (1997) and Lund and Zoback (1999).

the following, equivalent, results:

$$\frac{S_1 - P_f}{S_3 - P_f} = \left(\sqrt{\mu^2 + 1} + \mu\right)^2 \tag{5}$$

(Jaeger and Cook, 1979) and

$$\Delta S_{\text{brittle}} = \frac{2\mu}{\sqrt{\mu^2 + 1}}(\bar{S} - P_f) \tag{6}$$

Details of the derivation of these two equations from the Coulomb frictional-failure criterion are given in Appendix A. Either of these equations can be used to predict differential stress as a function of depth in a crust in frictional equilibrium. Eq. (6) implies that the maximum differential stress at failure, for a given mean stress, decreases with increasing fluid pressure. That is, under hydrostatic (low) fluid pressure conditions, the maximum differential stress withstandable before failure occurs is higher than under lithostatic (high) fluid pressures.

The three endmember stress configurations in which $S_1$, $S_2$, or $S_3$ is the vertical stress $S_v = \rho g z$, corresponding to normal, strike-slip and reverse faulting, respectively, give rise to similar explicit relations between depth and maximum differential stress:

$$\Delta S_{\text{brittle}} = \rho g z(\lambda - 1)(1 - F)/F \tag{7a}$$

$$\Delta S_{\text{brittle}} = 2\rho g z(\lambda - 1)(1 - F)/(1 + F) \tag{7b}$$

$$\Delta S_{\text{brittle}} = \rho g z(\lambda - 1)(1 - F) \tag{7c}$$

where $F$ is defined in Eq. (5), and

$$\lambda = \frac{P_f}{S_v} = \frac{P_f}{\rho g z} \tag{8}$$

$g$ is the gravitational acceleration, $\rho$ is the mean rock density, and $z$ is depth. Hence, for given stress and pore pressure regimes, we can estimate the maximum differential stress expected on the basis of the frictional-failure equilibrium hypothesis, and compare this with observational data.

## 3. Differential stress and pore pressure conditions in the brittle crust

In Section 2, it was noted that the brittle crust appears to be in a state of failure equilibrium. Here we briefly summarize data leading to this conclusion, and demonstrate the manner in which critically stressed faults control not only differential stress levels, but also pore pressures. Further details are given in Townend and Zoback (2000).

Stress data collected at several locations worldwide since the early 1980s indicate almost without exception that differential stresses increase with depth at gradients consistent with Eq. (5) for laboratory-measured coefficients of friction of 0.6–1.0 (Fig. 1). The solid lines are theoretical relationships representing Eq. (5) for various frictional coefficients: it is clear that the stress data from each deep borehole display the interdependency expected for critically stressed crust with frictional coefficients similar to those

Table 1
Locations exhibiting near-hydrostatic fluid pressures at depths of several kilometers. HDR — hot dry rock; DST — drill stem test; SWC — static water column; SG — silica geothermometry; N — normal stress regime; R — reverse stress regime; SS — strike-slip stress regime

| Well location | Stress regime | Depth (km) | Observation |
|---|---|---|---|
| Cornwall HDR, England[a] | SS | 2.5 | DST |
| Fenton Hill HDR, New Mexico[b] | N/SS | 3.0 | SWC |
| Dixie Valley, Nevada[c] | N | 2–3, 5–7 | DST, SG |
| Cajon Pass, California[d] | SS | 3.5 | DST |
| Soultz HDR, France[e] | N/SS | 5.0 | DST |
| Siljan, Sweden[f] | SS | 7.0 | DST |
| KTB, Germany[g] | SS | 9.1 | DST, SWC |
| Kola, Russia[h] | ?R | 12.2 | SWC |

[a] Pine et al. (1983).
[b] Barton et al. (1988).
[c] Hickman et al. (1997).
[d] Coyle and Zoback (1988).
[e] Baumgärtner et al. (1998).
[f] Lund and Zoback (1999).
[g] Huenges et al. (1997) and Zoback and Harjes (1997).
[h] Borevsky et al. (1987).

measured in laboratory experiments (Byerlee, 1978). The datasets presented in Fig. 1 are augmented by data from shallow depths in the crust (<3 km), which also substantiate the observation that the upper crust is critically stressed according to Coulomb frictional-failure theory (McGarr and Gay, 1978; Zoback and Healy, 1984, 1992).

Large-scale hydraulic tests and induced seismicity behavior at these and other locations at depths as great as 9 km demonstrate convincingly that upper crustal permeability is generally $10^{-17}$–$10^{-16}$ m$^2$ over lengthscales of 10–1000 m (Townend and Zoback, 2000) and that the associated pore pressures are very close to hydrostatic levels (Table 1). Geothermal and metamorphic data also suggest that the permeability of the upper crust exceeds $10^{-18}$ m$^2$ throughout the brittle crust (Manning and Ingebritsen, 1999).

Using data from the Cajon Pass, Long Valley and Yucca Mountain USW-G1 boreholes, Barton et al. (1995) demonstrated that optimally oriented planes are hydraulically conductive, whereas non-optimally oriented planes are non-conductive. That is, the faults that limit the crust's strength to that predicted using Coulomb frictional-failure theory, are also responsible for limiting pore pressures to hydrostatic values. The authors mapped fracture orientations, along the length of each borehole, and tested the hypothesis that optimally oriented faults are associated with localized thermal anomalies, and, by inference, with localized flow. The results (Fig. 2) clearly indicate that critically stressed faults act as fluid conduits and control large-scale permeability (Townend and Zoback, 2000). This conclusion is supported by data collected subsequently from boreholes in Dixie Valley, Nevada (Hickman et al., 1997; Barton et al., 1998). A similar result was obtained by Ito and Zoback (2000) for faults and fractures intersecting the Continental Deep Drilling Program (KTB; Kontinentales Tiefbohrprogramm der Bundesrepublik Deutschland) main borehole. The inset in Fig. 2 illustrates the combined datasets in terms of the ratio of shear stress to effective normal stress. It is apparent that the mean of this ratio is approximately 0.6 for the conductive fractures (consistent with Coulomb frictional-failure on well-oriented faults), and only ~0.3 for the non-conductive fractures (indicating that the fractures are not well oriented).

The characteristic diffusion time $\Omega$ for fluid of viscosity $\eta$ and compressibility $\beta_f$ to diffuse a distance $L$ through a porous medium with porosity $\varphi$ and compressibility $\beta_r$ is

$$\Omega = \frac{L^2}{\kappa} \approx \frac{(\varphi\beta_f + \beta_r)\eta L^2}{k} \tag{9}$$

where $\kappa \approx k/(\varphi\beta_f + \beta_r)\eta$ is the hydraulic diffusivity. For low-porosity rocks ($\varphi < 0.02$) at average temperatures of 150°C, $\beta_f = 4 \times 10^{-10}$ Pa$^{-1}$, $\beta_r = 2 \times 10^{-11}$ Pa$^{-1}$, and $\eta = 1.9 \times 10^{-4}$ Pa s, giving diffusion times of $\Omega$ = 10–1000 years over distances of 1–10 km, comparable to the thickness of the brittle crust (Townend and Zoback, 2000). The implication is, therefore, that over these intervals of time, pore pressures equilibrate, the crust is effectively permeable and deep crustal pore pressures are predominantly hydrostatic.

The resulting hydrostatic pore pressures enable faults to sustain high differential stresses before failure (as implied by Eq. (6)), making the brittle crust stronger than it would be if pore pressures were higher. In Section 4, we investigate what effect

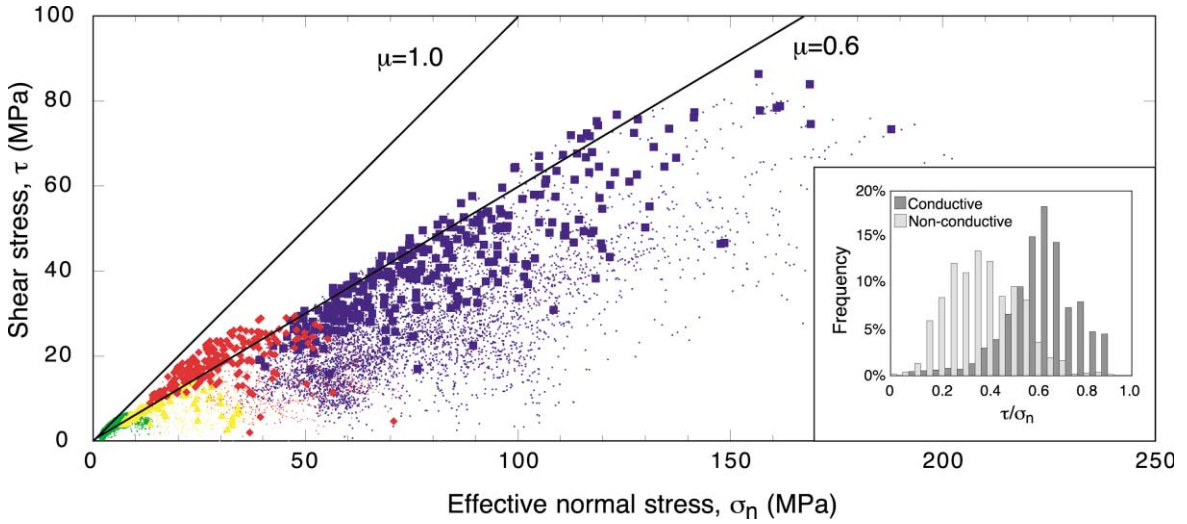


Fig. 2. Shear and effective normal stresses on fractures identified using borehole imaging techniques in the Cajon Pass (red diamonds and dots), Long Valley (yellow triangles and dots), Nevada Test Site (green circles and dots), and KTB (blue squares and dots) boreholes. The larger, filled symbols represent hydraulically conductive fractures and faults, and the dots represent non-conductive fractures. The inset figure illustrates the range in shear to normal stress ratio for all four datasets combined. The number of data in each dataset is normalized so that each dataset has equal weight. Original data from Barton et al. (1995) and Ito and Zoback (2000).

this high strength has on intraplate lithospheric deformation.

## 4. The effects of critical stress states and pore pressures on the strength and deformation of intraplate lithosphere

There is a relatively straightforward and intuitive reason why the brittle crust is in failure equilibrium. A force applied to the lithosphere causes the lower crust and upper mantle to undergo ductile deformation. Ongoing ductile creep loads the upper crust, eventually to the point of failure (Fig. 3). The amount of force that can be sustained by the upper crust is limited to its brittle strength, and any remaining force is available to cause ductile deformation of the lower crust and upper mantle. Hence, stress levels in the upper crust are controlled by its frictional strength, and lithospheric strain rates are controlled by the remaining force and the rheological parameters of the ductile lithosphere. If the brittle and ductile layers of intraplate lithosphere are coupled, then the entire lithosphere deforms at the same strain rate (Liu and Zoback, 1997).

We wish to investigate the roles played by upper crustal critical stress states and hydrostatic pore pressures in controlling the distribution of strength (integrated differential stress, Eq. (1)) in intraplate lithosphere and the rates at which intraplate

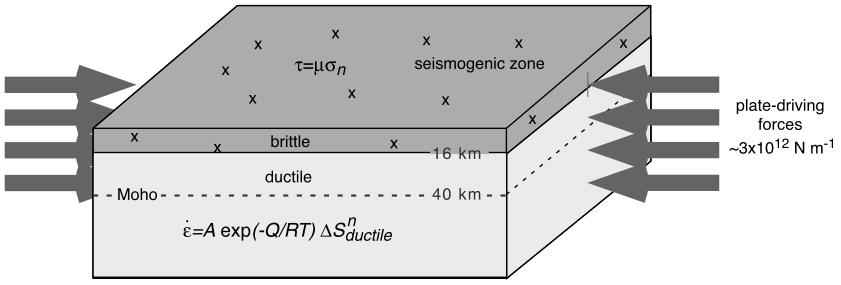


Fig. 3. Schematic illustration of the layered mechanical structure of continental lithosphere assumed for the strain rate calculations.

lithosphere deforms. Eqs. (7a)–(7c) enables us to estimate how differential stress increases with depth in the brittle crust based on the critical stress hypothesis. As is well known, at mid-crustal depths, however, the temperature is sufficiently high that ductile failure mechanisms are active at lower differential stress levels than required for brittle faulting (Sibson, 1983; Chen and Molnar, 1983; Kohlstedt et al., 1995). Following previous authors, we model the rheologies of the ductile crust and lithospheric mantle (Fig. 3) using a power-law creep relationship (e.g. Brace and Kohlstedt, 1980). In this case, the ductile strain rate $\dot{\varepsilon}$ is given in terms of the differential stress by

$$\dot{\varepsilon} = A \exp\left(-\frac{Q}{RT}\right)\Delta S^{n}_{\text{ductile}} \tag{10}$$

so that

$$\Delta S_{\text{ductile}} = \sqrt[n]{\frac{\dot{\varepsilon}}{A}\exp\left(\frac{Q}{RT}\right)} \tag{11}$$

Here $A$, $n$ and $Q$ are material parameters (the flow parameter, stress exponent and activation energy, respectively), $R$ is the gas constant and $T$ is the absolute temperature (Ranalli and Murphy, 1987). At any depth in the crust, we postulate that the rock deforms by whichever mechanism requires the lower differential stress, in which case

$$\Delta S = \min(\Delta S_{\text{brittle}}, \Delta S_{\text{ductile}}) \tag{12}$$

Clearly, $\dot{\varepsilon}$ is nonzero for any nonzero differential stress, and therefore even in the brittle regime a strain rate exists such that the rock deforms in a ductile form at a lower differential stress than required for brittle failure. However, by invoking the constraint that the total lithospheric strength be $3 \times 10^{12}$ N m$^{-1}$ and assuming that the upper crust, lower crust and lithospheric mantle are fully coupled, a single strain rate for the whole lithosphere can be found.

## 5. Modeling procedure

Our basic modeling procedure consists of first calculating the differential stresses required for brittle and ductile deformation separately, as functions of depth, and then combining the two profiles according to Eq. (12) to produce a composite differential stress profile. Integrating this profile over the thickness of the lithosphere gives the cumulative strength, which must equal $3 \times 10^{12}$ N m$^{-1}$. Note that this technique differs fundamentally from those of several other authors (e.g. Sibson, 1983; Ranalli and Murphy, 1987; Kohlstedt et al., 1995) in so far as that the lithospheric strain rate is a dependent variable and not a free parameter.

A generalized lithospheric structure composed of a 16 km-thick felsic upper crust (with rheological properties of dry Adirondack granulite), 24 km-thick mafic lower crust (dry Pikwitonei granulite), and 60 km-thick lithospheric mantle (wet Aheim dunite) is assumed, based on the composite velocity-depth model obtained by Christensen and Mooney (1995) and rheological coefficients from Carter and Tsenn (1987) and Wilks and Carter (1990). In a semi-infinite layered half-space with zero temperature at the surface, the steady-state temperature profile is given by

$$T(z) = \sum_{i=1}^{N}\left[\frac{q_{i-1}\Delta z_i}{K_i} - \frac{H_i \Delta z_i^2}{2K_i}\right] \tag{13}$$

The volumetric heat production, thermal conductivity, thickness and basal heat flow of the $i$th layer are $H_i$, $K_i(T)$, $\Delta z_i$ and $q_i = q_{i-1} - H_i \Delta z_i$, respectively. We have incorporated a very simple heat productivity model, in which the heat productivities of the upper crust, lower crust and lithospheric mantle are constant (cf. Pollack and Chapman, 1977; Chapman and Furlong, 1992), and equal to 1.1, 0.40 and 0.02 $\mu$W m$^{-3}$, respectively (Jaupart et al., 1998; Rudnick et al., 1998). We assume thermal conductivity to be a function of both temperature and depth, according to relations presented by Chapman and Furlong (1992) and Schatz and Simmons (1972).

Continental-scale stress mapping (Zoback and Zoback, 1980, 1989, 1991; Zoback, 1992) indicates that stable continental lithosphere typically exhibits oblique strike-slip stress states (i.e. $S_2 = S_v$). We have incorporated a strike-slip stress state in the modeling, with the additional assumption that $S_2 = \bar{S}$. In this case, differential stress is given as a function of depth by Eq. (7b).

We treat pore pressures in the lower crust as near-lithostatic, following the arguments presented by Nur and Walder (1990). At elevated temperatures,

Table 2
Values of the parameters used in the lithospheric strength calculations. Asterisks ( $*$ ) indicate those parameters that were varied in the Monte Carlo routine: each parameter was drawn at random from a specific normal distribution with the listed mean ($\bar{x}$) and standard deviation ($\sigma$) such that $3\sigma = 0.2\bar{x}$, giving approximately $\pm 20\%$ variation

| Parameter (symbol) | Value | Units |
|---|---|---|
| Density ($\rho$) | 2800 | kg m$^{-3}$ |
| Coefficient of friction ($\mu$) | 0.8$^*$ | – |
| Thickness ($z$) | | |
| Upper crust | 16 | km |
| Lower crust | 24 | km |
| Lithospheric mantle | 60 | km |
| Conductivity ($K$) | | |
| Upper crust (nominal) | 3.0$^*$ | W m$^{-1}$ K$^{-1}$ |
| Lower crust (nominal) | 2.6$^*$ | W m$^{-1}$ K$^{-1}$ |
| Lithospheric mantle (nominal) | 3.4$^*$ | W m$^{-1}$ K$^{-1}$ |
| Heat productivity ($H$) | | |
| Upper crust | 1.1 | $\mu$W m$^{-3}$ |
| Lower crust | 0.4 | $\mu$W m$^{-3}$ |
| lithospheric mantle | 0.02 | $\mu$W m$^{-3}$ |
| Flow parameter ($A$) | | |
| Upper crust | 0.08$^*$ | MPa$^{-n}$ s$^{-1}$ |
| Lower crust | 12589$^*$ | MPa$^{-n}$ s$^{-1}$ |
| Lithospheric mantle | 398$^*$ | MPa$^{-n}$ s$^{-1}$ |
| Stress exponent ($n$) | | |
| Upper crust | 3.1$^*$ | – |
| Lower crust | 4.2$^*$ | – |
| Lithospheric mantle | 4.5$^*$ | – |
| Activation energy ($Q$) | | |
| Upper crust | 243$^*$ | kJ mol$^{-1}$ |
| Lower crust | 445$^*$ | kJ mol$^{-1}$ |
| Lithospheric mantle | 498$^*$ | kJ mol$^{-1}$ |

processes of permeability reduction by chemical precipitation and inelastic deformation are expected to occur at rates sufficient to preclude rapid fluid migration, and hence to favor high pore pressures. Specifically, the permeability of the lower crust probably does not exceed $10^{-19}$ m$^2$ at 30 km depth (Manning and Ingebritsen, 1999) implying long characteristic diffusion times ($>10^5$ years) such that near-lithostatic pore pressures are likely to be maintained.

Given the temperature–depth profile and an initial estimate of the ductile strain rate, $\dot{\varepsilon}$, we can calculate differential stresses in the ductile portion of the upper and lower crust and lithospheric mantle using Eq. (11). However, the strain rate calculations involve several parameters whose values are nonunique (such as surface heat flow, conductivity, upper crustal heat productivity, the frictional coefficient, and the rheological parameters of each layer). We have investigated the effects of variations in each of these parameters using a Monte Carlo technique: 1000 estimates of each parameter are drawn at random from normal distributions and 1000 separate models constructed, so that the $j$th model is a function of $q_0(j)$, $K(j)$, $\mu(j)$, etc. Finally, composite temperature–depth, differential stress–depth and strength–depth profiles are constructed by stacking the different models' results. The values of the modeling parameters are listed in Table 2.

To summarize, we wish to calculate a single lithospheric strain rate such that the integral of the differential stress profile is equal to the postulated strength of the lithosphere, namely $3 \times 10^{12}$ N m$^{-1}$. To accommodate uncertainties in the input parameters, we perform 1000 Monte Carlo simulations: for each simulation, we iteratively adjust the strain rate until the strength criterion is met.

## 6. Model limitations

We have opted to treat the ductile behavior of the lithosphere as being dominated by dislocation (power-law) creep, and have not incorporated diffusion (linear) creep into the models. Karato and Wu (1993) suggested that diffusion creep may occur in the shallow asthenospheric mantle beneath continental lithosphere but noted that several parameters, particularly grain size and the dislocation creep activation volume, make it difficult to accurately determine the depths at which each mechanism dominates. We have consequently neglected diffusional effects in the interests of simplicity.

Additionally, we have used thermal parameters considered representative of stable continental crust, and a correspondingly representative lithospheric structure. However, the rheologies of the lower crust and mantle are poorly known. For example, if the mantle had the rheology of dry Aheim dunite — for which $A = 32\,000$ MPa$^{-n}$ s$^{-1}$, $Q = 498$ kJ mol$^{-1}$ and $n = 3.6$, (Carter and Tsenn, 1987) — rather than wet,

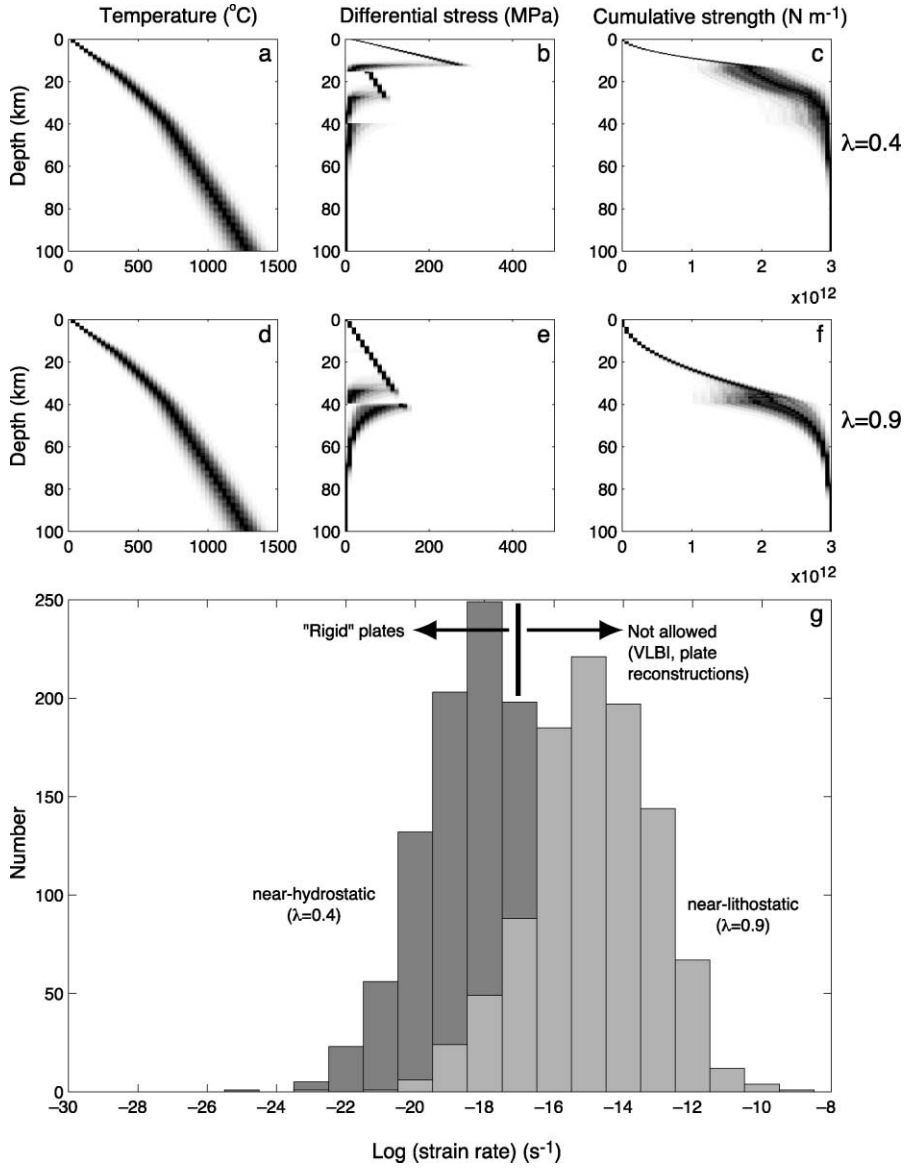


Fig. 4. Results of 1000 Monte Carlo calculations for a strike-slip stress state and surface heat flow of 60 ± 6 mW $m^{-2}$, subject to the constraint that the total strength of the lithosphere is $3 \times 10^{12}$ N $m^{-1}$. (a), (b), and (c) are the temperature, differential stress, and cumulative strength profiles respectively under near-hydrostatic upper crustal pore pressure conditions ($\lambda = 0.4$), and (d), (e), and (f) are the corresponding profiles under near-lithostatic conditions ($\lambda = 0.9$). (g) illustrates the range of calculated lithospheric strain rates under each condition.

it would deform much less rapidly for a given differential stress. Furthermore, the strength of the lower crust is modeled here assuming near-lithostatic pore pressures in the lower crust.

Our modeling procedure accommodates variation in several of the input parameters (as listed in Table 2) but we have not allowed the strength constraint to vary. $3 \times 10^{12}$ N $m^{-1}$ is an intermediate estimate of the strength of the lithosphere (see Kusznir, 1991) and we have decided to fix this value in order to facilitate interpretation of the differential stress and strength profiles.

## 7. Results

Fig. 4 illustrates the modeling results corresponding to surface heat flow of $60 \pm 6$ mW m$^{-2}$ (mean $\pm$ 10%), representative of stable continental heat flow (data from Pollack et al., 1993). The uppermost plots (a–c) display the model results assuming hydrostatic pore pressures in the upper crust (for which $\lambda$ defined in Eq. (8) is approximately 0.4), and the three middle plots (d–f) display the corresponding results for near-lithostatic pore pressures ($\lambda = 0.9$). Note that the temperature–depth profiles are the same in both cases. At the bottom of the figure is a histogram (g) illustrating the range of estimated strain rates under each pore pressure condition: the strain rates are distributed log-normally. Strain rates are distributed about a geometric mean of approximately $10^{-18}$ s$^{-1}$ under near-hydrostatic upper crustal pore pressure conditions. In comparison, under near-lithostatic pore pressures, the average strain rate is approximately $10^{-15}$ s$^{-1}$.

Additionally, differences in the distribution of strength within the lithosphere can be clearly observed by comparing plots (c) and (f). For the strike-slip stress state and hydrostatic pore pressures, the 16 km-thick upper crust provides $\sim 1.5 \times 10^{12}$ N m$^{-1}$ (1/2) of the total lithospheric strength, whereas it accounts for $\sim 0.5 \times 10^{12}$ N m$^{-1}$ (1/6) under near-lithostatic pore pressures.

The significance of the strain rate results can be appreciated by comparing them with the value of $10^{-17}$ s$^{-1}$ given above for the maximum intraplate strain rate. On the basis of our models, strain rates under near-hydrostatic upper crustal pore pressure conditions and stress and thermal regimes characteristic of intraplate regions are likely to be less than $10^{-17}$ s$^{-1}$, whereas they are likely to substantially exceed $10^{-17}$ s$^{-1}$ under near-lithostatic pore pressure conditions. The latter rates are greater than those observed in stable continental lithosphere and it therefore appears that the lithosphere's rigidity may be controlled by upper crustal pore pressures.

Note, however, that for lower surface heat flows of $50 \pm 5$ mW m$^{-2}$ — such as are typical of Proterozoic and Archean cratonic crust (after Pollack et al., 1993) — strain rates are lower than $10^{-20}$ s$^{-1}$ under either pore pressure regime. We suggest, therefore, that in intraplate regions with other than very low heat flow, hydrostatic pore pressures in the upper crust give the lithosphere sufficient rigidity for plate tectonics to occur. In low heat-flow regions of stable continental crust, pore pressures do not seem to play a significant role in determining lithospheric strain rates.

## 8. Conclusions

Numerous data obtained from deep boreholes worldwide reveal that upper crustal permeabilities are sufficiently high ($10^{-17}$–$10^{-16}$ m$^2$) that pore pressures attain hydrostatic values over geologically short periods of time (10–1000 years). These high permeabilities appear to be maintained by hydraulically conductive, critically stressed faults. Such faults limit the strength of the brittle crust and, since the ductile lithosphere is postulated to deform at any finite differential stress, the strength of the lithosphere as a whole. Given therefore that the crust is both critically stressed *and* capable of sustaining tectonic stresses of approximately $3 \times 10^{12}$ N m$^{-1}$, the strength of intraplate lithosphere must equal the imposed plate tectonic stress.

We have used a total force constraint on models of lithospheric strength profiles to determine at what strain rates intraplate lithosphere deforms. We estimate that under strike-slip stress regimes and thermal conditions representative of stable continental regions, hydrostatic upper crustal pore pressures are associated with strain rates of less than $10^{-17}$ s$^{-1}$, whereas lithostatic pore pressures produce unrealistically high strain rates: the lithosphere cannot deform more rapidly than approximately $10^{-17}$ s$^{-1}$ or lithospheric plates would not be sufficiently rigid for plate tectonic processes to occur on time scales of millions of years. We conclude, therefore, that hydrostatic pore pressures in the upper crust are necessary in other than very low heat flow regions for the lithosphere to deform sufficiently slowly that plates behave as if rigid, and hence for plate reconstructions to be possible.

## Acknowledgements

We thank Terry Engelder, Steve Miller, and Jean-Louis Vigneresse for their constructive reviews of this work. Financial support of the National Science

Foundation (Award 96-14267) is gratefully acknowledged. John Townend is supported by an Arco Stanford Graduate Fellowship.

## Appendix A

### A.1. Stress relations for a critically stressed fault

To obtain Eq. (5), we substitute Eqs. (2) and (3) into the Coulomb frictional-failure criterion, Eq. (4):

$$\tau = \mu\sigma_n$$

$$\frac{S_1 - S_3}{2}\sin 2\theta = \mu\left[\frac{S_1 + S_3 - 2P_f}{2} + \frac{S_1 - S_3}{2}\cos 2\theta\right]$$

which we rearrange to give

$$\frac{S_1 - P_f}{S_3 - P_f} = \frac{\sin 2\theta + \mu(1 - \cos 2\theta)}{\sin 2\theta - \mu(1 + \cos 2\theta)}$$

$$= \frac{\cos\phi + \mu(1 + \sin\phi)}{\cos\phi - \mu(1 - \sin\phi)}$$

since $\phi = 2\theta - \pi/2$ for a critically stressed fault. Next, $\mu = \tan\phi$, so that $\sin\phi = \mu/\sqrt{\mu^2 + 1}$ and $\cos\phi = 1/\sqrt{\mu^2 + 1}$, in which case the relation simplifies to

$$\frac{S_1 - P_f}{S_3 - P_f} = \frac{\sqrt{\mu^2 + 1} + \mu}{\sqrt{\mu^2 + 1} - \mu} = 1 + 2\mu^2 + 2\mu\sqrt{\mu^2 + 1}$$

$$= \left(\sqrt{\mu^2 + 1} + \mu\right)^2$$

as required.

Likewise, we can obtain Eq. (6) by expressing Eqs. (2) and (3) in terms of the differential and mean stresses,

$$\tau = \frac{\Delta S_{\text{brittle}}}{2}\sin 2\theta$$

and

$$\sigma_n = \bar{S} - P_f + \frac{\Delta S_{\text{brittle}}}{2}\cos 2\theta$$

On substituting $\tau$ and $\sigma_n$ into Eq. (4) and simplifying we obtain

$$\Delta S_{brittle} = \frac{2\mu}{\sin 2\theta - \mu\cos 2\theta}(\bar{S} - P_f)$$

where, as above, we can rewrite the equations in terms of $\phi$, and make use of the trigonometric relationships between $\phi$ and $\mu$ to give

$$\Delta S_{\text{brittle}} = \frac{2\mu}{\sqrt{\mu^2 + 1}}(\bar{S} - P_f)$$

### A.2. Stress–depth relations for critically stressed crust

Eqs. (7a)–(7c) can be obtained by substituting the appropriate expressions for $S_1$ and $S_3$ (listed below) into Eq. (5) and rearranging

- normal — $S_1 = S_v = \rho gz$, $S_3 = \rho gz - \Delta S_{\text{brittle}}$
- strike-slip — $S_2 = S_v = \rho gz$, $S_1 = \rho gz + \Delta S_{\text{brittle}}/2$, $S_3 = \rho gz - \Delta S_{\text{brittle}}/2$
- reverse — $S_3 = S_v = \rho gz$, $S_1 = \rho gz + \Delta S_{brittle}$.

## References

Anderson, J.G., 1986. Seismic strain rates in the central and eastern United States. Bull. Seismol. Soc. Am. 76, 273–290.

Barton, C.A., Zoback, M.D., Burns, K.L., 1988. In situ stress orientation and magnitude at the Fenton Hill geothermal site, New Mexico, determined wellbore breakouts. Geophys. Res. Lett. 15, 467–470.

Barton, C.A., Zoback, M.D., Moos, D., 1995. Fluid flow along potentially active faults in crystalline rock. Geology 23, 683–686.

Barton, C.A., Hickman, S.H., Morin, R., Zoback, M.D., Benoit, D., 1998. Reservoir-scale fracture permeability in the Dixie Valley, Nevada, geothermal field. Abstracts Volume, Society of Petroleum Engineers Annual Meeting, Trondheim, Paper Number 47371, pp. 315–322.

Batchelor, A.S., Pine, R.J., 1986. The results of in situ stress determinations by seven methods to depths of 2500 m in the Carnmenellis granite. Proceedings of the International Symposium on Rock Stress and Rock Stress Measurements, Stockholm, pp. 467–478.

Baumgärtner, J., Gérard, A., Baria, R., Jung, R., Tran-Viet, T., Gandy, T., Aquilina, L., Garnish, J., 1998. Circulating the HDR reservoir at Soultz: maintaining production and injection flow in complete balance, initial results of the 1997 circulation experiment. Twenty-third Workshop on Geothermal Reservoir Engineering, Stanford, pp. 11–20.

Borevsky, L.V., Vartanyan, G.S., Kulikov, T.B., 1987. Hydrogeological essay. In: Kozlovsky, Y.A. (Ed.), The Superdeep Well of the Kola Peninsula. Springer, New York, pp. 271–287.

Bott, M.H.P., Kusznir, N.J., 1984. The origin of tectonic stress in the lithosphere. Tectonophysics 105, 1–13.

Brace, W.F., Kohlstedt, D., 1980. Limits on lithospheric stress

imposed by laboratory measurements. J. Geophys. Res. 85, 6248–6252.
Brudy, M., Zoback, M.D., Fuchs, K., Rummel, F., Baumgärtner, J., 1997. Estimation of the complete stress tensor to 8 km depth in the KTB scientific drill holes: implications for crustal strength. Geophys. Res. 102, 18453–18475.
Byerlee, J.D., 1978. Friction of rocks. Pure Appl. Geophys. 116, 615–626.
Carter, N.L., Tsenn, M.C., 1987. Flow properties of continental lithosphere. Tectonophysics 136, 27–63.
Chapman, D.S., Furlong, K.P., 1992. Thermal state of the continental lower crust. In: Fountain, D.M., Arculus, R., Kay, R.W. (Eds.), Continental Lower Crust. Elsevier, Amsterdam, pp. 179–199.
Chen, W.-P., Molnar, P., 1983. Focal depths of intracontinental and intraplate earthquakes and their implications for the thermal and mechanical properties of the lithosphere. J. Geophys. Res. 88, 4183–4214.
Christensen, N.I., Mooney, W.D., 1995. Seismic velocity structure and composition of the continental crust: a global view. J. Geophys. Res. 100, 9761–9788.
Coyle, B.J., Zoback, M.D., 1988. In situ permeability and fluid pressure measurements at ~2 km depth in the Cajon Pass research well. Geophys. Res. Lett. 15, 1029–1032.
England, P.C., Houseman, G.A., 1986. Finite strain calculations of continental deformation. 2. Comparison with the India–Asia collision zone. J. Geophys. Res. 91, 3664–3676.
Forsyth, D., Uyeda, S., 1975. On the relative importance of the driving forces of plate motion. Geophys. J. R. Astron. Soc. 43, 163–200.
Gordon, R.G., 1998. The plate tectonic approximation: plate nonrigidity, diffuse plate boundaries, and global plate reconstructions. Annu. Rev. Earth Planet. Sci. 26, 615–642.
Hickman, S.H., Barton, C.A., Zoback, M.D., Morin, R., Sass, J., Benoit, R., 1997. In situ stress and fracture permeability along the Stillwater fault zone Dixie Valley, Nevada. Int. J. Rock Mech. Min. Sci. 34 (126), 414.
Houseman, G.A., England, P.C., 1986. Finite strain calculations of continental deformation. 1. Method and general results for convergent zones. J. Geophys. Res. 91, 3651–3663.
Hubbert, M.K., Rubey, W.W., 1959. Role of fluid pressure in the mechanics of overthrust faulting. Geol. Soc. Am. Bull. 70, 115–205.
Huenges, E., Erzinger, J., Kück, J., Engeser, B., Kessels, W., 1997. The permeable crust: geohydraulic properties down to 9101 m depth. J. Geophys. Res. 102, 18255–18265.
Ito, T., Zoback, M.D., 2000. Fracture permeability and in situ stress to 7km depth in the KTB scientific drillhole. Geophys. Res. Lett. 27, 1045–1048.
Jaeger, J.C., Cook, N.G.W., 1979. Fundamentals of Rock Mechanics. Chapman & Hall, London 593pp.
Jaupart, C., Mareschal, J.C., Guillou-Frottier, L., Davaille, A., 1998. Heat flow and thickness of the lithosphere in the Canadian Shield. J. Geophys. Res. 103, 15269–15286.
Karato, S., Wu, P., 1993. Rheology of the upper mantle: a synthesis. Science 260, 771–778.
Kohlstedt, D.L., Evans, B., Mackwell, S.J., 1995. Strength of the lithosphere: constraints imposed by laboratory experiments. J. Geophys. Res. 100, 17587–17602.
Kusznir, N.J., 1991. The distribution of stress with depth in the lithosphere: thermo-rheological and geodynamic constraints. In: Whitmarsh, R.B. (Ed.), Tectonic Stress in the Lithosphere. Royal Society, London, pp. 95–107.
Liu, L., Zoback, M.D., 1997. Lithospheric strength and intraplate seismicity in the New Madrid seismic zone. Tectonics 16, 585–595.
Lund, B., Zoback, M.D., 1999. Orientation and magnitude of in situ stress to 6.5 km depth in the Baltic Shield. Int. J. Rock Mech. Min. Sci. 36, 169–190.
Manning, C.E., Ingebritsen, S.E., 1999. Permeability of the continental crust: implications of geothermal data and metamorphic systems. Rev. Geophys. 37, 127–150.
McGarr, A., Gay, N.C., 1978. State of stress in the earth's crust. Annu. Rev. Earth Planet. Sci. 6, 405–436.
McNutt, M.K., 1984. Lithospheric flexure and thermal anomalies. J. Geophys. Res. 89, 1180–1194.
Nur, A., Walder, J., 1990. Time-dependent hydraulics of the earth's crust. In: Bredehoeft, J.D., Norton, D.L. (Eds.), The Role of Fluids in Crustral Processes. National Academy Press, Washington, DC, pp. 113–127.
Pine, R.J., Ledingham, P., Merrifield, C.M., 1983. In situ stress measurement in the Carnmenellis Granite. II. Hydrofracture tests at Rosemanowes Quarry to depths of 2000 m. Int. J. Rock Mech. Min. Sci. 20, 63–72.
Pollack, H.N., Chapman, D.S., 1977. On the regional variation of heat flow, geotherms and lithosphere thickness. Tectonophysics 38, 279–296.
Pollack, H.N., Hurter, S.J., Johnson, J.R., 1993. Heat flow from the Earth's interior; analysis of the global data set. Rev. Geophys. 31, 267–280.
Raleigh, C.B., Healy, J.H., Bredehoeft, J.D., 1972. Faulting and crustal stress at Rangely, Colorado. Am. Geophys. Union Monogr. 16, 275–284.
Ranalli, G., Murphy, D.C., 1987. Rheological stratification of the lithosphere. Tectonophysics 132, 281–295.
Roeloffs, E., 1996. Poroelastic techniques in the study of earthquake-related hydrologic phenomena. Adv. Geophys. 37, 135–195.
Rudnick, R.L., McDonough, W.F., O'Connell, R.J., 1998. Thermal structure, thickness and composition of continental lithosphere. Chem. Geol. 145, 395–411.
Schatz, J.P., Simmons, G., 1972. Thermal conductivity of earth materials at high temperatures. J. Geophys. Res. 77, 6966–6983.
Sibson, R.H., 1974. Frictional constraints on thrust, wrench and normal faults. Nature 249, 542–544.
Sibson, R.H., 1983. Continental fault structure and the shallow earthquake source. J. Geol. Soc. Lond. 5, 741–767.
Simpson, D.W., Leith, W.S., Scholz, C.H., 1988. Two types of reservoir-induced seismicity. Bull. Seismol. Soc. Am. 78, 2025–2040.
Stein, R.S., King, G.C., Lin, J., 1992. Change in failure stress on the southern San Andreas fault system caused by the 1992 magnitude = 7.4 Landers earthquake. Science 258, 1328–1332.
Stein, R.S., Barka, A.A., Dieterich, J.H., 1997. Progressive failure

on the North Anatolian fault since 1939 by earthquake stress triggering. Geophys. J. Int. 128, 594–604.

Townend, J., Zoback, M.D., 2000. How faulting keeps the crust strong. Geology 28, 399–402.

Wilks, K.R., Carter, N.L., 1990. Rheology of some continental lower crustal rocks. Tectonophysics 182, 57–77.

Zoback, M.D., Harjes, H.-P., 1997. Injection-induced earthquakes and crustal stress at 9 km depth at the KTB deep drilling site, Germany. J. Geophys. Res. 102, 18477–18491.

Zoback, M.D., Healy, J.H., 1984. Friction, faulting and in situ stress. Ann. Geophys. 2, 689–698.

Zoback, M.D., Healy, J.H., 1992. In situ stress measurements to 3.5 km depth in the Cajon Pass scientific research borehole: implications for the mechanics of crustal faulting. J. Geophys. Res. 97, 5039–5057.

Zoback, M.D., Zoback, M.L., 1991. Tectonic stress field of North America and relative plate motions. In: Slemmons, D.L., Engdahl, E.R., Zoback, M.D., Blackwell, M.L. (Eds.), Neotectonics of North America. Geol. Soc. Am., Boulder, CO, 339–366.

Zoback, M.L., 1992. First and second order patterns of stress in the lithosphere: the World Stress Map Project. J. Geophys. Res. 97, 11703–11728.

Zoback, M.L., Zoback, M.D., 1980. State of stress in the conterminous United States. J. Geophys. Res. 85, 6113–6156.

Zoback, M.L., Zoback, M.D., 1989. Tectonic stress field of the conterminous United States. Geol. Soc. Am. Mem. 172, 523–539.